High-resolution crystal structure of copper amine oxidase from *Arthrobacter globiformis*: assignment of bound diatomic molecules as O_2

Takeshi Murakawa,[a] Hideyuki Hayashi,[b] Tomoko Sunami,[c] Kazuo Kurihara,[c] Taro Tamada,[c] Ryota Kuroki,[c] Mamoru Suzuki,[d] Katsuyuki Tanizawa[e] and Toshihide Okajima[e]*

[a]Department of Biochemistry, Osaka Medical College, 2-7 Daigakumachi, Takatsuki, Osaka 569-8686, Japan, [b]Department of Chemistry, Osaka Medical College, 2-7 Daigakumachi, Takatsuki, Osaka 569-8686, Japan, [c]Molecular Structural Biology Group, Quantum Beam Science Directorate, Japan Atomic Energy Agency, 2-4 Shirakata-Shirane, Tokai, Ibaraki 319-1195, Japan, [d]Institute for Protein Research, Osaka University, 3-2 Yamadaoka, Suita, Osaka 565-0871, Japan, and [e]The Institute of Scientific and Industrial Research, Osaka University, 8-1 Mihogaoka, Ibaraki, Osaka 567-0047, Japan

Correspondence e-mail: tokajima@sanken.osaka-u.ac.jp

The crystal structure of a copper amine oxidase from *Arthrobacter globiformis* was determined at 1.08 Å resolution with the use of low-molecular-weight polyethylene glycol (LMW PEG; average molecular weight ∼200) as a cryoprotectant. The final crystallographic R factor and R_{free} were 13.0 and 15.0%, respectively. Several molecules of LMW PEG were found to occupy cavities in the protein interior, including the active site, which resulted in a marked reduction in the overall B factor and consequently led to a subatomic resolution structure for a relatively large protein with a monomer molecular weight of ∼70 000. About 40% of the presumed H atoms were observed as clear electron densities in the $F_o - F_c$ difference map. Multiple minor conformers were also identified for many residues. Anisotropic displacement fluctuations were evaluated in the active site, which contains a post-translationally derived quinone cofactor and a Cu atom. Furthermore, diatomic molecules, most likely to be molecular oxygen, are bound to the protein, one of which is located in a region that had previously been proposed as an entry route for the dioxygen substrate from the central cavity of the dimer interface to the active site.

1. Introduction

Copper amine oxidases (CuAOs) catalyze the oxidative deamination of various primary amines to produce the corresponding aldehydes, hydrogen peroxide and ammonia. In CuAOs occurring widely in both prokaryotes and eukaryotes (McIntire & Hartmann, 1993; Klema & Wilmot, 2012), a Cu^{2+} ion and a quinone cofactor abbreviated as topa quinone or TPQ (2,4,5-trihydroxyphenylalanine quinone) are contained in the active site (Janes *et al.*, 1990). Physiologically, prokaryotic CuAOs are mostly inducible enzymes produced for the assimilation of primary amines as carbon and nitrogen sources. In eukaryotes, they are involved in various cellular processes. An animal enzyme designated diamine oxidase detoxifies various bioactive amines, including histamine (Maintz & Novak, 2007). Lysyl oxidases belonging to the CuAO family react with the side chains of protein lysine residues to form cross-links in collagen molecules (Lucero & Kagan, 2006). Moreover, through the production of H_2O_2 by amine oxidation, CuAOs contribute to cell death, vascular adhesion of lymphocyte cells and adipocyte maturation in animals (Hernandez *et al.*, 2006; Jalkanen *et al.*, 2007) and germination, root growth and healing of cell-wall wounds in plants (Cona *et al.*, 2006).

It has been well established that the organic cofactor TPQ is post-translationally synthesized from a specific tyrosine residue encoded in the polypeptide chain of all CuAOs (Matsuzaki *et al.*, 1994; Klinman & Mu, 1994; Choi *et al.*, 1995;

Okajima & Tanizawa, 2009). TPQ biosynthesis is a self-catalytic process requiring only molecular oxygen and Cu. In contrast to free TPQ, which is very labile in aqueous and aerobic solutions, the cofactor TPQ exists stably by being accommodated in the buried active site of CuAOs (Okajima & Tanizawa, 2009). After the single-turnover formation of TPQ, the mature enzyme can then catalyze the multi-turnover reaction of amine oxidation. The catalytic reaction consists of an initial reductive half-reaction involving two-election reduction of the oxidized form of TPQ by the amine substrate and a subsequent oxidative half-reaction involving the re-oxidation of the reduced form of TPQ by molecular oxygen, employing a ping-pong mechanism for substrate binding and product release. Thus, molecular oxygen is essential for both cofactor biogenesis and catalysis.

The X-ray crystal structures of CuAOs determined to date include those from *Escherichia coli* (ECAO; Parsons *et al.*, 1995), pea seedling (Kumar *et al.*, 1996), *Arthrobacter globi-formis* (AGAO; Wilce *et al.*, 1997), the yeast *Hansenula polymorpha* (Li *et al.*, 1998), *Pichia pastoris* (lysyl oxidase; Duff *et al.*, 2003), human [vascular adhesion protein 1 (Airenne *et al.*, 2005) and diamine oxidase (McGrath *et al.*, 2009)], bovine serum (Lunelli *et al.*, 2005) and *Aspergillus nidulans* (McGrath *et al.*, 2011). All are homodimers containing a 70–95 kDa subunit with very similar chain folding consisting of the three common domains D2, D3 and D4, with the exception of ECAO which has an extra N-terminal D1 domain. Domains D2 (residues 9–91 in AGAO) and D3 (residues 103–203) wrap a large core consisting of two D4 domains (residues 229–623) in the dimer (Supplementary Fig. S1*a*[1]). A large solvent-filled central cavity, termed the 'inland lake' (Duff *et al.*, 2003, 2004), lies between the two D4 domains (Supplementary Fig. S1*b*). TPQ is contained in each D4 domain and is buried about 12 Å (in AGAO) from the molecular surface. There is a channel between the D3 and D4 domains through which substrate amines enter the active site (Wilce *et al.*, 1997; Matsuzaki & Tanizawa, 1998). A conserved tyrosine residue (Tyr296 in AGAO) located at the bottom of the channel is likely to act as a 'gate' (Wilce *et al.*, 1997) to the active site (Supplementary Figs. S1*b* and 1*c*). The prosthetic metal, Cu^{2+}, is coordinated by the imidazole rings of three conserved histidine residues (His431, His433 and Hi592 in AGAO) by Cu^{2+}—N bonds of about 2.0 Å in length. The entry route for molecular oxygen has been suggested to be either from the internal lake *via* a short polar channel or from either end of the *β*-sandwich of the D4 domain through an internal hydrophobic region (Wilce *et al.*, 1997; Lunelli *et al.*, 2005; McGrath *et al.*, 2011; Duff *et al.*, 2004; Johnson *et al.*, 2007; Pirrat *et al.*, 2008).

We initially determined the crystal structure of AGAO at 2.2 Å resolution using diffraction data obtained at 298 K (PDB entry 1av4; Wilce *et al.*, 1997) and subsequently at 1.8 Å resolution using data obtained at 100 K (PDB entry 1iu7;

Kishishita *et al.*, 2003). More recently, Langley and coworkers determined the structure of AGAO at 1.55 Å resolution (PDB entry 1w6g) at 100 K using glycerol-protected crystals prepared under different crystallization conditions (Langley *et al.*, 2006). We have also solved several structures of AGAO as TPQ biogenesis intermediates (Kim *et al.*, 2002) and catalytic intermediates (Chiu *et al.*, 2006; Murakawa *et al.*, 2006, 2012; Taki *et al.*, 2008). The resolutions of all these AGAO structures were around 1.5 Å at best; the highest resolution among the crystal structures of CuAOs determined to date is that of *P. pastoris* lysyl oxidase solved at 1.23 Å (Duff *et al.*, 2006).

In this study, using low-molecular-weight polyethylene glycol (LMW PEG; average molecular weight ∼200) as a cryoprotectant, we determined the crystal structure of AGAO at 1.08 Å resolution. The binding of several molecules of LMW PEG onto the protein surface and, more importantly, within the protein interior resulted in a significant reduction in the displacement fluctuation of the whole molecule and thereby provided a diffraction data set at subatomic resolution. As the most prominent finding, we identified four diatomic molecules that were assigned as being most likely to be molecular oxygen in the AGAO crystals prepared under atmospheric conditions. This is the first crystallographic identification of molecular oxygen bound to a CuAO. In addition, the refined model provided information on aniso-tropic displacement parameters and multiple minor conformers for a large number of residues as well as experimentally determined coordinates of about 40% of the H atoms.

2. Materials and methods

2.1. Enzyme expression and purification

E. coli CD03, a mutant strain of *E. coli* BL21(DE3) with two disrupted catalase genes (Kishishita *et al.*, 2003), carrying the expression vector pEPO-02 encoding AGAO was cultivated in a Cu-depleted medium. The Cu^{2+}/TPQ-free apo form of the enzyme was purified to homogeneity as described previously (Matsuzaki *et al.*, 1994). The purity was judged to be >99% by SDS–PAGE. The Cu^{2+}/TPQ-containing holo form of AGAO was prepared by dialysis of the apoenzyme against 3 l 50 m*M* HEPES buffer pH 6.8 containing 50 µ*M* $CuSO_4$ at 277 K for 48 h followed by dialysis against 3 l of 50 m*M* HEPES buffer pH 6.8 containing 1 m*M* ethylenediaminetetraacetic acid at 277 K for 24 h to remove unbound or weakly bound Cu^{2+} ions. Protein concentrations were determined spectrophoto-metrically using an extinction coefficient at 280 nm of 13.2 for a 1%(*w*/*v*) solution (Matsuzaki *et al.*, 1994) and were expressed as subunit concentrations unless otherwise stated.

2.2. Crystallization

AGAO was crystallized by the microdialysis method as described previously (Kishishita *et al.*, 2003). The enzyme solution (10 mg ml⁻¹) was placed in a 50 µl dialysis button and dialyzed at 289 K against 1.05 *M* potassium sodium tartrate in 25 m*M* HEPES buffer pH 6.8 in a normal atmosphere or an N_2 atmosphere (a glove box filled with N_2 gas). Single crystals

Table 1
Statistics of data collection and crystallographic refinement.

Values in parentheses are for the highest resolution shell.

	Crystal grown in a normal atmosphere (AGAO$_{PG}$)	Crystal grown in an N$_2$ atmosphere (AGAO$_{N2}$)
Data collection		
Temperature (K)	100	100
Wavelength (Å)	0.9000	0.9000
Space group	$C2$	$C2$
Unit-cell parameters (Å, °)	a = 157.7, b = 62.4, c = 92.1, β = 112.1	a = 191.6, b = 63.0, c = 158.0, β = 117.4
No. of molecules per asymmetric unit	1	2
No. of observations	2710201	1138063
No. of unique reflections	663537	232158
Multiplicity	4.1	5.0
Resolution range (Å)	50–1.08 (1.10–1.08)	50–1.55 (1.61–1.55)
Completeness (%)	96.5 (63.3)	95.4 (95.5)
R_{merge}† (%)	6.2 (44.4)	12.5 (49.9)
Average $I/\sigma(I)$	42.3 (2.12)	31.6 (3.14)
Wilson B factor (Å^2)	9.9	15.8
Refinement statistics		
Resolution range (Å)	35.01–1.08	29.93–1.55
No. of protein atoms per asymmetric unit	9579/4876‡	9752
No. of solvent atoms	905	1709
R.m.s. deviation from ideal values		
Bond lengths (Å)	0.011	0.013
Bond angles (°)	1.58	1.58
Isotropic average B factor (Å^2)		
Protein	17.3/15.6‡	20.1
Ligand/ion	33.6/30.4‡	35.6
Water	31.8	34.2
R factor§ (%)	13.0	18.1
R_{free}¶ (%)	15.0	21.0
Ramachandran plot statistics (%)		
Residues in favoured regions	96.7	96.3
Residues in allowed regions	3.0	3.2
Outliers	0.3	0.5

† $R_{merge} = \sum_{hkl}\sum_i |I_i(hkl) - \langle I(hkl)\rangle| / \sum_{hkl}\sum_i I_i(hkl)$, where $I_i(hkl)$ is an individual intensity measurement and $\langle I(hkl)\rangle$ is the average intensity for this reflection. ‡ The second value is excluding H atoms. § $R = \sum_{hkl} ||F_{obs}| - |F_{calc}|| / \sum_{hkl} |F_{obs}|$. ¶ R_{free} is an R factor for the refinement evaluated using 5% of the reflections, which were excluded from the refinement.

with approximate dimensions of 0.4 × 0.8 × 0.3 mm grew in about two weeks. After sufficient growth of the crystals in the normal and N$_2$ atmospheres, the dialysis buttons were transferred into new reservoirs, where the solutions were supplemented with 35%(v/v) LMW PEG as a cryoprotectant and kept at 289 K for 24 h for cryoprotection. For the crystals in the N$_2$ atmosphere, the same PEG solution for cryoprotection was pre-equilibrated overnight in the glove box to remove dissolved dioxygen. The crystals were mounted on thin nylon loops (diameter 0.4–0.5 mm) and cooled by flash-cooling them to 100 K in a cold N$_2$ gas stream or by soaking then in liquid CF$_4$ for crystals obtained in a normal atmosphere or in an N$_2$ atmosphere, respectively.

2.3. Data collection and refinement

X-ray diffraction data were collected at 100 K with synchrotron radiation (wavelength 0.9 Å) using an MX-225HE detector (Rayonix, Evanston, Illinois, USA) on

beamline BL44XU and a Quantum315r detector (ADSC, California, USA) on beamline BL38B1 at SPring-8, Hyogo, Japan for single crystals grown in a normal and an N$_2$ atmosphere, respectively. To cover the entire range of intensities, the subatomic resolution data were collected as two sets of diffraction measurements with differing crystal-to-detector distances (105 and 220 mm) for the crystal grown in a normal atmosphere. The data for the crystal grown in an N$_2$ atmosphere were collected with a single crystal-to-detector distance of 150 mm. The sets of diffraction data collected from the same crystal were processed and scaled using *HKL*-2000 (Otwinowski & Minor, 1997). R_{merge} was calculated from unmerged data and R_{merge} > 50% was used to define the resolution-limit cutoff (Table 1). Crystals grown in both normal and N$_2$ atmospheres were found to belong to space group $C2$, but with different unit-cell pamameters (see §3). The details and statistics of data collection are summarized in Table 1. The phase was determined by molecular replacement using *Phaser* v.2.5.0 (McCoy *et al.*, 2007). *REFMAC* v.5.5 (Murshudov *et al.*, 2011) and *CNS* v.1.2 (Brünger *et al.*, 1998) were used for initial refinement, calculation of electron-density maps and assignment of solvent molecules. Model building and validation were performed with *Coot* v.0.6.2 (Emsley *et al.*, 2010). The AGAO structure (PDB entry 1iu7) which had been determined at 1.8 Å resolution using diffraction data from crystals cryoprotected with glycerol and assigned as space group $I2$, equivalent to space group $C2$ (Kishishita *et al.*, 2003), was used as a search model in the molecular replacement. In the search model, chain A of 1iu7 was selected without solvent molecules and TPQ382 was replaced by an unmodified Tyr residue. The initial structure obtained by molecular replacement (without ligands and water molecules) was subjected to rigid-body refinement and was further refined by simulated annealing with slow cooling from 2500 to 300 K with a 25 K decrease per cycle and several cycles of B-factor and positional refinement. The residue at position 382 was replaced by TPQ based on $2F_o - F_c$, $F_o - F_c$ and OMIT maps. Metal ions, water molecules and LMW PEG molecules were assigned on the basis of the highest peaks in the respective $2F_o - F_c$ maps. The assignment of diatomic molecules is described in §3. Initial coordinates and cif format library files of the ligands were obtained from the database of *Coot*. Further refinement was performed with *PHENIX* v.1.8 (Adams *et al.*, 2010). The metal-site stereochemistry was refined without any restraints. For the high-resolution structure of the crystal grown in a normal atmosphere, H atoms in the protein molecules and LMW PEG molecules were added automatically. This model was refined through several further cycles of B-factor, occupancy and positional refinement after correction of solvent molecules. During the final stages of refinement, anisotropic B factors were applied to the non-H atoms. The Ramachandran plot was calculated using *MolProbity* (Chen *et al.*, 2010) for structure validation. The details and statistics of the crystallographic refinements are also summarized in Table 1. *UCSF Chimera* v.1.6 (Pettersen *et al.*, 2004) and *PyMOL* v.1.3 (Schrödinger) were used for graphical preparation of the X-ray crystal structures. The

atomic coordinates and structure factors of the AGAO structures determined for the crystals grown in the normal and N_2 atmospheres have been deposited in the Protein Data Bank with accession codes 3wa2 and 3wa3, respectively.

3. Results

3.1. Effects of LMW PEG on AGAO crystals

Previously, an AGAO crystal at 298 K ($AGAO_{RT}$) was found to belong to space group $C2$, with unit-cell parameters $a = 158.65$, $b = 64.57$, $c = 93.29$ Å, $\beta = 113.49°$ (PDB entry 1av4; Wilce *et al.*, 1997), while an AGAO crystal at 100 K ($AGAO_{GL}$) also belonged to space group $C2$ but with different unit-cell parameters: $a = 192.96$, $b = 62.63$, $c = 157.52$ Å, $\beta = 117.68°$ (Kishishita *et al.*, 2003). The former small $C2$ unit cell contained a monomer in the asymmetric unit, whereas the latter unit cell had a twofold volume containing a dimer in the asymmetric unit. The conversion of

the unit cell resulted from a slight deviation of the twofold crystallographic axis from the b axis upon soaking of the crystals in 45%(v/v) glycerol for 16 h (Kishishita *et al.*, 2003). Although the recent AGAO structure determined at cryo-temperature with glycerol (PDB entry 1w6g; Langley *et al.*, 2006; $AGAO_{GL2}$) had unit-cell parameters similar to those of $AGAO_{RT}$, it appeared to be likely that the use of glycerol as a cryoprotectant slightly affected the crystal packing or symmetry. Thus, to avoid this type of side effect, we surveyed other cryoprotectants and found that LMW PEG with an average molecular weight of about 200 was suitable as a good cryoprotectant for AGAO crystals.

After the AGAO crystals had been soaked with 35%(v/v) LMW PEG for 16 h, diffraction data were collected at 100 K using synchrotron radiation. Most of the crystals were found to belong to space group $C2$, with a small unit cell comparable to those of $AGAO_{RT}$ (Wilce *et al.*, 1997; Supplementary Table S1). However, crystals belonging to a large $C2$ unit cell comparable to those of $AGAO_{GL}$ (Kishishita *et al.*, 2003) were
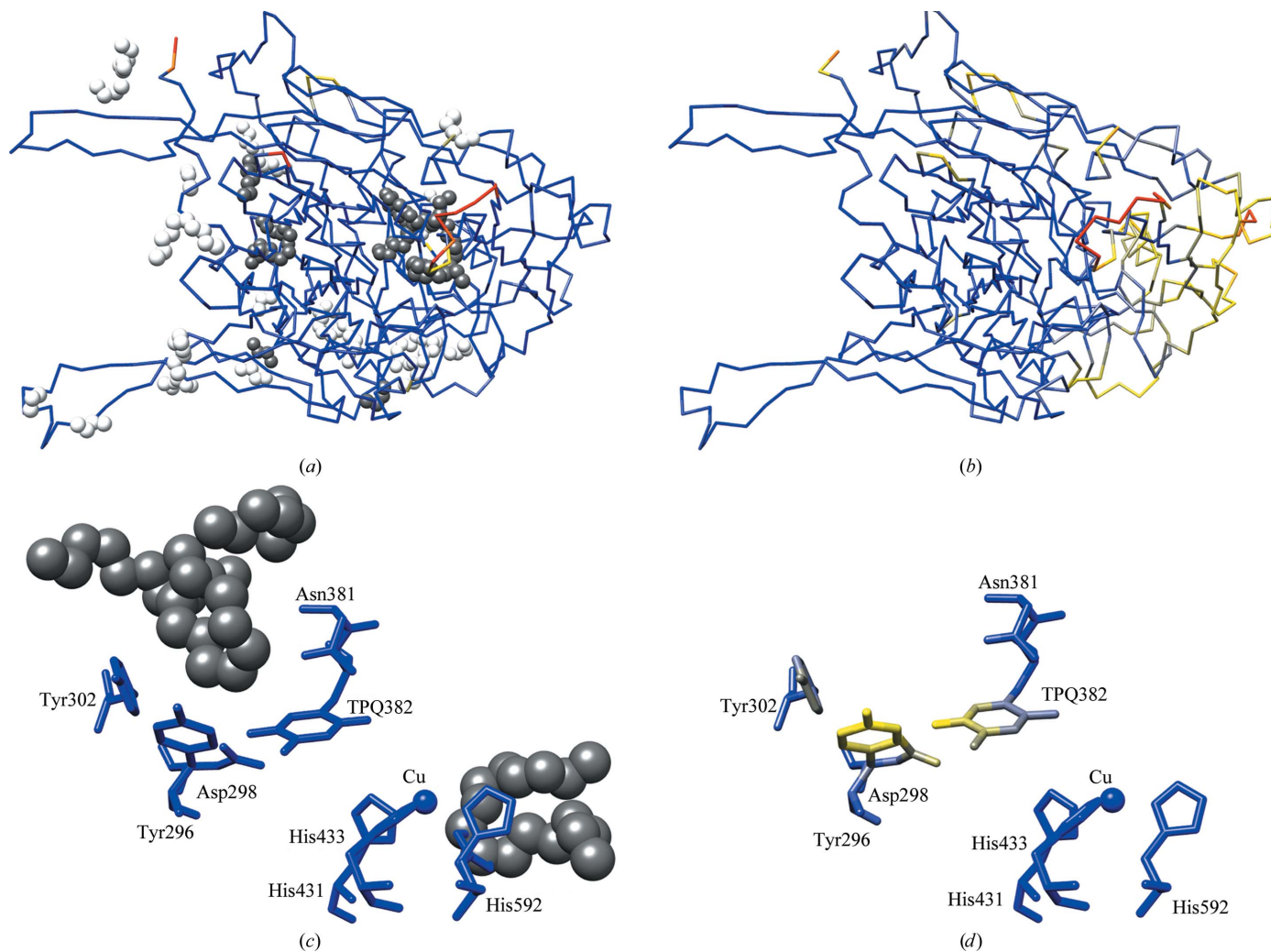
Figure 1
Comparison of low-resolution and high-resolution AGAO structures. The isotropic B factors for (*a*) $AGAO_{PG}$ and (*b*) $AGAO_{GL}$ are shown on ribbon models of the main-chain structure using a rainbow colour gradation from blue (15 Å^2) to red (65 Å^2). Close-up views of the active site are shown in (*c*) and (*d*) for $AGAO_{PG}$ and $AGAO_{GL}$, respectively. In (*a*) and (*d*), LMW PEGs bound to the surface and in the interior of the protein are shown as light and dark grey spheres, respectively.

also occasionally observed. The crystals with the small unit cell were found to provide higher resolution diffraction data than those with the large unit cell. The processed data set for one of the crystals with the small unit cell (designated $AGAO_{PG}$) reached a subatomic resolution of 1.08 Å. This resolution is quite high for a relatively large protein with a monomer molecular weight of ~70 000; $AGAO_{PG}$ is second to the highest resolution crystal structure of a 210 kDa homotrimeric enzyme, endosialidase NF, which diffracted to 0.98 Å resolution (Schulz *et al.*, 2010).

Among the $AGAO_{RT}$, $AGAO_{GL}$, $AGAO_{GL2}$ and $AGAO_{PG}$ crystals (Supplementary Table S1), $AGAO_{PG}$ has the smallest unit-cell volume and the lowest solvent content. The decreases in the unit-cell volume and solvent content correlate well with the diffraction resolution of these crystals. A dehydration effect (Heras & Martin, 2005) provided by LMW PEG together with the binding of a number of LMW PEG molecules to the protein surface and interior (see below) presumably caused the crystals to shrink, with closer crystal packing and better ordering of the protein molecules. Crystal shrinkage owing to dehydration caused by various compounds including ethylene glycol and PEG 400 has also been reported for several proteins (Heras & Martin, 2005). In addition, the B factor of $AGAO_{PG}$ (9.9 Å^2) obtained from the Wilson plot (Winn *et al.*, 2011) was found to be significantly lower than those of $AGAO_{GL}$ (18.0 Å^2) and $AGAO_{RT}$ (23.7 Å^2) (Supplementary Table S1). The drastic decrease in the B factor is consistent with the decrease in the isotropic B factors obtained from the solved structure as described below.

3.2. Overall structure and small molecules

The phase problem of the data set processed at 1.08 Å resolution was solved by molecular replacement with the AGAO monomer and the model was further refined to give the final crystallographic R factor and R_{free} values shown in Table 1. The polypeptide chain of the final model is composed of residues 9–629; eight N-terminal and nine C-terminal residues were excluded because of the absence of corresponding electron density. The isotropic B factors of the main-chain atoms of $AGAO_{PG}$ are markedly lower than those of $AGAO_{GL}$, especially in the D2 and D3 domains (Figs. 1a and 1b and Supplementary Fig. S2), likely owing to the binding of a number of LMW PEG molecules in the intra-protein and inter-protein spaces and the resultant reduction of thermal fluctuation of flexible regions as described below. Exceptionally, a loop region (residues 50–56) exhibits very poor electron density. This loop protrudes from the D2 domain and is not involved in the interactions with adjacent molecules in the crystal packing; therefore, it has high flexibility. The active-site residues such as Tyr296, Asp298, Tyr302, Asn381 and TPQ382 also have smaller isotropic B factors in $AGAO_{PG}$ (Fig. 1c) than in $AGAO_{GL}$ (Fig. 1d).

In the $F_o - F_c$ difference map, peaks of residual electron density with a level higher than 1.0σ were assigned as H atoms. Fig. 2 exemplifies a region with residual electron densities that are unambiguously assignable to H atoms (His586–Gly589).

Similarly, about 40% of all of the presumed H atoms were observed in the monomer molecule. Identification of these H atoms correlates with the isotropic B factors of the heavier atoms to which the H atoms are covalently attached; most of the identified H atoms are attached to atoms with an isotropic B factor of about 15 Å^2 or less.

A total of 905 water molecules and 29 LMW PEG molecules with different chain lengths [12, nine, five, one and two molecules of $HO-(CH_2CH_2-O)_n-H$, where n = 1, 2, 3, 4 and 5, respectively; Fig. 1a] were assigned in the model on the basis of the high-resolution electron-density map. Among the bound LMW PEG molecules, 19 of them are located on the protein surface and ten in the protein interior. They were found either in the inland lake (three molecules) or in the inter-domain clefts (four in a narrow cleft between the D2 and D4 domains and three in the amine channel between the D3 and D4 domains; Figs. 1a and 1c), where water molecules were bound in the previous $AGAO_{GL}$ structure (Kishishita *et al.*, 2003). Several molecules of LMW PEG bound on the protein surface, particularly on the surface of the D2 and D3 domains, are located between the symmetry molecules in the crystal packing, leading to a significant reduction in the isotropic B factors of these domains. As LMW PEG was later added to the crystals as a cryoprotectant, these results show that LMW PEG molecules could diffuse into the crystal lattice and were bound to the protein without damaging the crystal structure and packing.

Besides the active-site Cu^{2+} ion, a metal ion with a strong electron density was found on the protein surface and was coordinated by the side-chain carboxyl groups of Asp440 and Asp581, the main-chain carbonyl groups of Ile582 and Met441 and a water molecule (Supplementary Fig. S3). Among the metal ions contained in the crystallization buffer, an Na$^+$ ion better fitted to the electron density than a K$^+$ ion when the $F_o - F_c$ maps calculated by introducing a K$^+$ or an Na$^+$ ion into
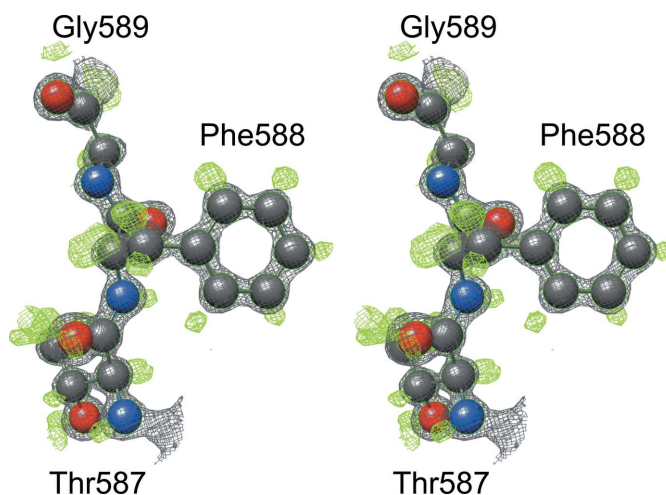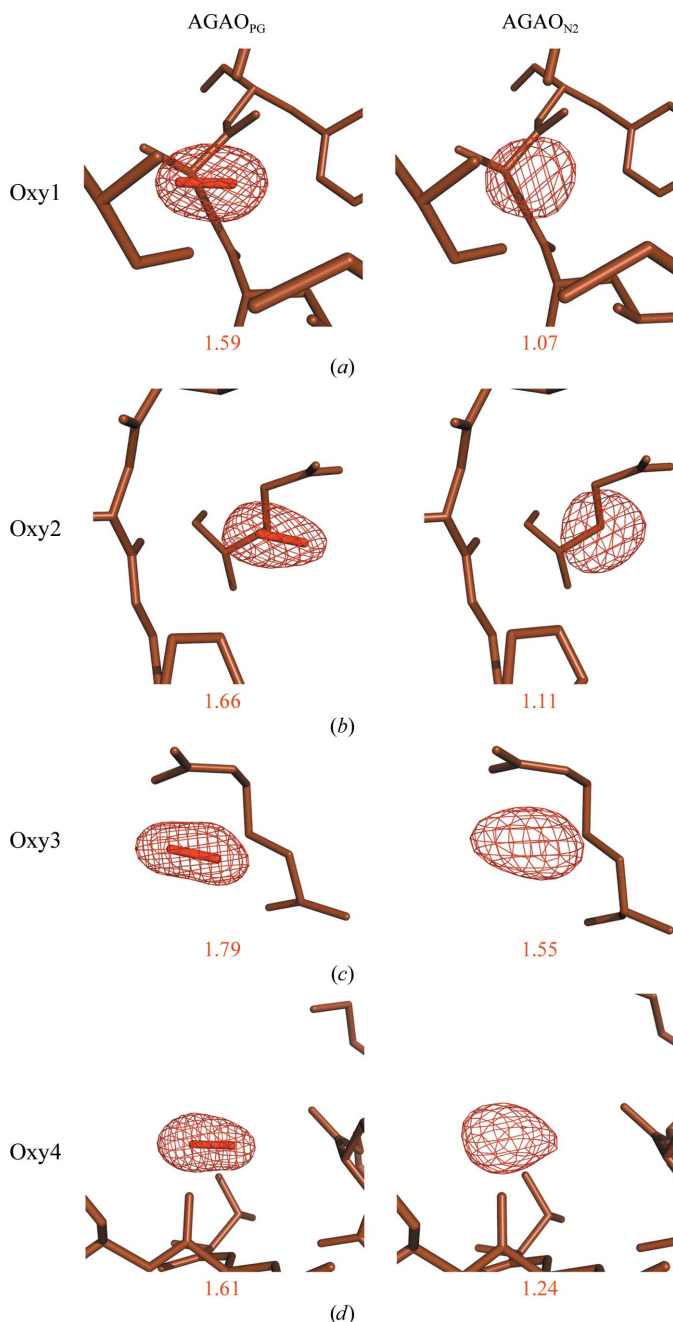

Figure 2
Electron densities for H atoms. The $2F_o - F_c$ map for amino-acid residues Thr587–Gly589 of $AGAO_{PG}$ is contoured at 3.0σ with a grey mesh on a stereo diagram of the ball-and-stick model. The $F_o - F_c$ map calculated by omitting the H atoms is contoured at 2.5σ with a green mesh.

the model were compared. Furthermore, the metal-coordination distances to main-chain carbonyl groups (2.5 Å), carboxyl groups (2.4 Å) or the water molecule (2.7 Å) were more preferable for Na^+ than for K^+ (Harding, 2006). In the structures of $AGAO_{GL2}$ (Langley *et al.*, 2006) and ECAO (Smith *et al.*, 2010), an Na^+ and a Ca^{2+} ion is bound in this site, respectively, whereas this site is vacant in $AGAO_{RT}$ (Wilce *et al.*, 1997) and $AGAO_{GL}$ (Kishishita *et al.*, 2003). The second Cu^{2+} ion identified in the vicinity of Asp161, Asp165, His170

and His201 located on the protein surface of $AGAO_{GL2}$ (Langley *et al.*, 2006) is replaced by a water molecule in $AGAO_{PG}$. Presumably, the weakly bound Cu^{2+} and Ca^{2+} ions, if any, had been removed by extensive dialysis against the buffer containing EDTA or diethyldithiocarbamate (a strong Cu chelator) during enzyme preparation and subsequent crystallization in the present study.

3.3. Assignment of diatomic molecules as molecular oxygen

During the assignment of water molecules, we noted the presence of residual electron densities with an ellipsoidal shape at various positions in the $2F_o - F_c$ and $F_o - F_c$ maps of $AGAO_{PG}$. To identify the molecule corresponding to these electron densities, several models were introduced on the basis of $2F_o - F_c$, $F_o - F_c$ and OMIT maps. A model of a water molecule with a single or double conformer could be fitted to the majority of the electron densities. However, electron densities at four particular positions were invalid for a water molecule, *i.e.* the electron density was too high to fit with a single O atom. Alternatively, the model of a diatomic gaseous molecule, such as N_2 or O_2, fitted well to these four ellipsoidal electron densities (designated Oxy1–4; Figs. 3 and 4). Similar ellipsoidal electron densities were also detected in the OMIT map calculated from the diffraction data sets at 1.14 and 1.21 Å resolution collected from different crystals which were grown in a normal atmosphere and cryoprotected with LMW PEG (data not shown). The diatomic molecules may be assignable as O_2 or N_2, since both occur at high concentrations in the normal atmosphere. Indeed, their models fitted well to the ellipsoidal electron densities with restraints. Furthermore, to assign the diatomic molecules as either O_2 or N_2, we determined the structure of AGAO crystals grown in an N_2 atmosphere ($AGAO_{N2}$), although it was technically difficult to optimize the soaking conditions (excess soaking of AGAO crystals with LMW PEG often causes crystal cracking) and to vitrify the the crystals without damaging them in a glove box filled with N_2 gas. Hence, even the best data set did not reach the subatomic resolution of $AGAO_{N2}$, which was found to belong to space group $C2$ with large unit-cell parameters (Table 1) comparable with those of $AGAO_{GL}$ (Kishishita *et al.*, 2003). It is probable that subtle damage (if any) and/or different crystal-preparation methods affected the molecular symmetry, resulting in the conversion to the large $C2$ unit cell. Nevertheless, the corresponding electron densities at these sites (Oxy1–4) were rather spherical except for Oxy3 in $AGAO_{N2}$ (Fig. 3); no significant residual electron density was observed in the $F_o - F_c$ map when a single water molecule was modelled for Oxy1, Oxy2 and Oxy4. These findings strongly suggest that the ellipsoidal electron densities observed at the Oxy1, Oxy2 and Oxy4 sites in the crystal grown in a normal atmosphere are assigned as O_2 molecules weakly bound to AGAO crystals, which are replaced by water on growing the crystal in an N_2 atmosphere. The diatomic molecule found at the Oxy3 site of $AGAO_{PG}$ could not be finally assigned as either O_2 or N_2, leaving a possibility that the O_2 (or N_2) bound

Figure 3
Electron densities corresponding to the diatomic molecules assigned as O_2. The $F_o - F_c$ OMIT maps for Oxy1 (*a*), Oxy2 (*b*), Oxy3 (*c*) and Oxy 4 (*d*) are contoured at 4σ with a red mesh calculated for $APAO_{PG}$ and $APAO_{N2}$. Numbers indicate the ellipsoidal indices (the ratio of the longest and the shortest axes) of the electron densities.

in a normal atmosphere was replaced by N_2 or was not replaced by water in an N_2 atmosphere.

Notwithstanding the possibility of N_2 binding at the Oxy3 site, O_2 molecules were finally modelled for these electron densities with a fixed occupancy of 100%. Two of them (Oxy1

and Oxy2) are located in the protein interior and the other two (Oxy3 and Oxy4) are near the subunit boundary on the surface of the dimer. Oxy1 is bound in a hydrophobic cavity formed by Trp118, Leu156, Ala157, Phe158, Val172, Leu175 and Ile290 inside the D3 domain (Fig. 4b). Apparently, no channel or route from this Oxy1-binding site to the active site is present. In contrast, Oxy2 is bound to a less hydrophobic site consisting of Glu399, His517, Thr606, Val607 and Gly608 together with several water molecules (Fig. 4c). The Oxy2 binding site is present on a route from the central cavity (inland lake) to the active site, which has been proposed as one of the possible entry pathways for the substrate dioxygen (Wilce et al., 1997; Lunelli et al., 2005; McGrath et al., 2011; Duff et al., 2004). In the conserved β-sandwich, another candidate for the dioxygen pathway (Johnson et al., 2007; Pirrat et al., 2008), no bound dioxygen molecule was identified. On the other hand, Oxy3 (either O_2 or N_2) is located near the dimer interface and is surrounded by Arg490, Glu486*, Ala487*, Asp488*, Asp540* (where an asterisk denotes a residue from another subunit of the dimer) and diethyleneglycol [HO–$(CH_2CH_2$–O$)_n$–H, n = 2] bound in this region (Fig. 4d). Oxy4 is also close to the dimer interface and appears to be stuck in a small hollow formed by Thr521, Leu522, Leu523, Ala537, Thr538, Ly539 and Arg457* (Fig. 4e). Both Oxy3 and Oxy4 are distant from either of the proposed dioxygen pathways. The binding of Oxy2, Oxy3 and Oxy4 to less hydrophobic sites is stabilized by hydrogen bonds and/or van der Waals interactions with nearby water molecules and amino-acid side chains. Relative orientations and hydrogen-bonding distances between the modelled dioxygen and water molecules (Fig. 4) coincide well with the theoretically calculated values for the van der Waals complex of O_2 and H_2O (Sabu et al., 2005).

Collectively, the final model consists of residues 9–629 of the AGAO monomer, one Cu atom, one Na atom, 29 molecules of LMW PEG, four molecules of dioxygen (or three O_2 plus one N_2) and 905 water molecules. The overall structure of $AGAO_{PG}$ is essentially identical to those of $AGAO_{GL}$
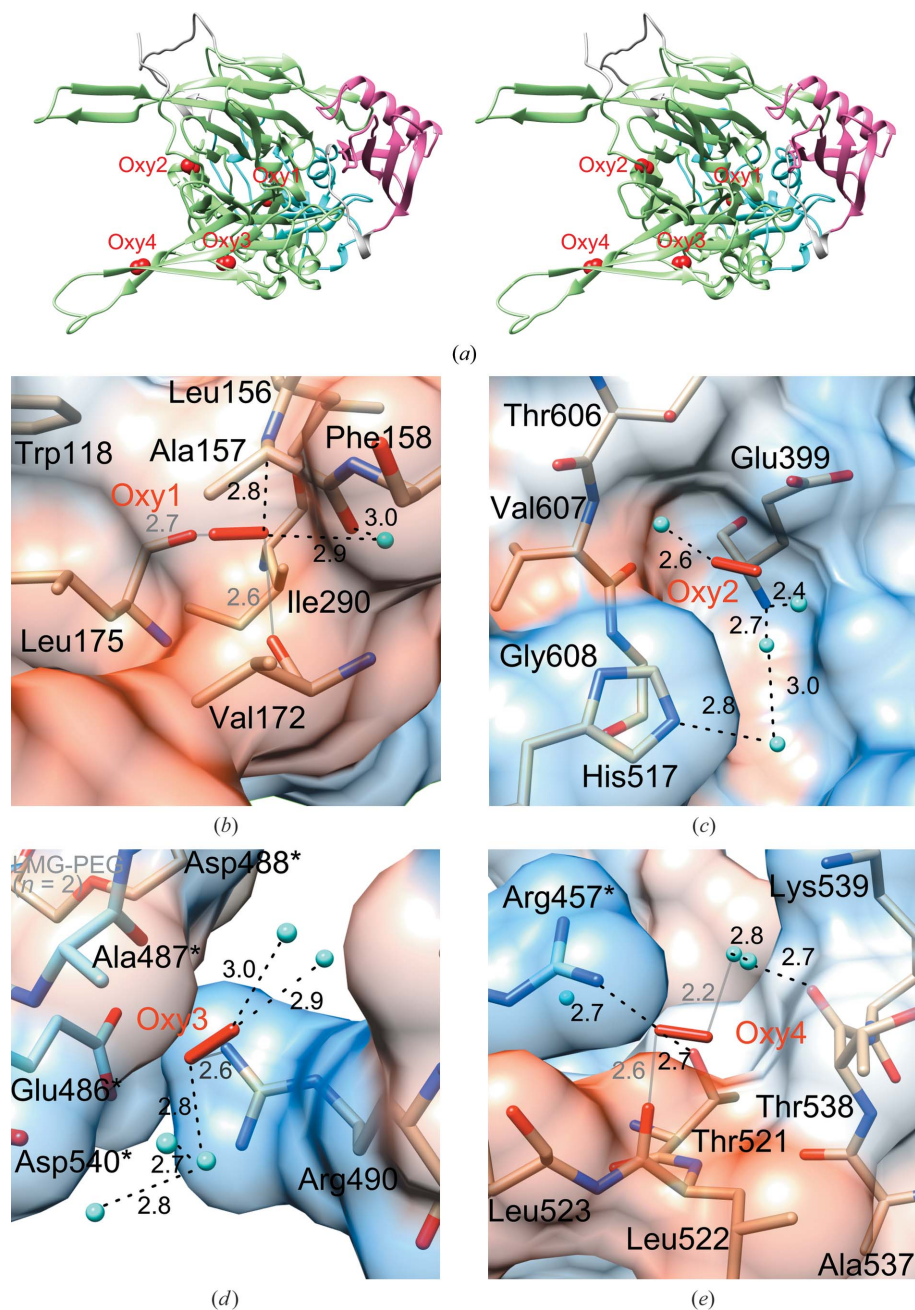
Figure 4
Localization of bound O_2-like diatomic molecules. (a) Refined models of molecular O atoms are shown as red spheres in a stereo diagram of the $AGAO_{PG}$ monomer (sky blue, D2; pink, D3; green, D4; grey, loops connecting domains). (b)–(e) The binding sites of Oxy1 (b), Oxy2 (c), Oxy3 (d) and Oxy4 (e) are depicted. Water molecules are represented as small cyan spheres. Amino-acid residues close to the bound dioxygen are shown in stick representation. The hydrophobicity of the surface was calculated with kdHydrophobicity (Kyte & Doolittle, 1982) and is represented by a colour graduation from blue (hydrophilic) to orange (hydrophobic). Presumed hydrogen-bonding and van der Waals interactions are shown as black dotted lines and grey solid lines, respectively, with the distances between two atoms labelled in Å.

and AGAO$_{RT}$, with root-mean-square deviations for C$^\alpha$ atoms of 0.41 and 0.53 Å, respectively.

3.4. Active-site structure

In the crystal structures of CuAOs determined previously, the quinone cofactor TPQ was found to have two distinct conformations (Parsons *et al.*, 1995; Wilce *et al.*, 1997; Duff *et al.*, 2003). In the catalytically inactive 'on-copper' conformation, the C4 hydroxyl group of TPQ is directed towards the Cu atom, replacing the axially coordinated water (Wat$_{ax}$). In the catalytically active 'off-copper' conformation, the C4 hydroxyl group of TPQ hydrogen bonds to a highly conserved Tyr residue (Tyr284 in AGAO) and the C2 carbonyl O atom interacts indirectly with the Cu atom *via* the axially coordinated water (Wat$_{ax}$). Reflecting this conformational flexibility, TPQ was often disordered in the crystal structures, with an unclear electron density in the $2F_o - F_c$ map (Parsons *et al.*, 1995; Wilce *et al.*, 1997). Even in AGAO$_{GL2}$ determined at 1.55 Å resolution, the electron density for TPQ382 was poor and was not assignable to a single conformation; the on-copper to off-copper conformation ratio was estimated to be 0.33:0.67 (Langley *et al.*, 2006). In AGAO$_{PG}$, however, the electron density for TPQ in the OMIT map contoured at 6σ is very clear (Supplementary Fig. S4) and reveals that TPQ adopts a single off-copper conformation (Fig. 5). Another conformer of TPQ is still undetectable in the OMIT map contoured at as low as 2σ. The C4 hydroxyl group of TPQ is strongly hydrogen bonded to the C4 hydroxyl group of Tyr284 at a distance of 2.58 Å, tethering the off-copper conformation. Nevertheless, no clear electron density for the H atoms on the ring C3 and C6 atoms is observed in the $F_o - F_c$ difference map because of the relatively large isotropic B factors of the TPQ ring (8.5–13.3 Å^2; average 11.3 Å^2). Likewise, H atoms are unobservable for the carboxyl and methylene groups of

Figure 5
Active-site structure. The active-site residues around TPQ and the Cu atom are shown as a stick model. The $F_o - F_c$ OMIT map for LMW PEGs and His592 is contoured at 3.0σ as a sky blue mesh. Cu atoms and water molecules are represented as orange and cyan spheres, respectively. Coordination bonds to Cu are represented by thin red lines and a hydrogen bond between TPQ382 and Tyr284 is represented by a black broken line labelled with the distance between two atoms.
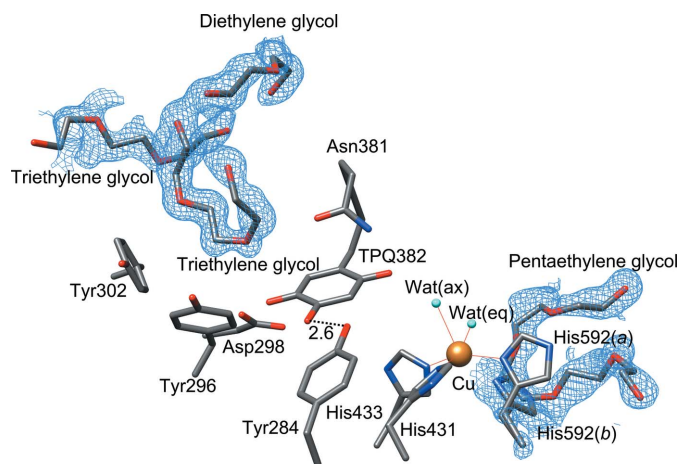
Asp298, which acts as an essential catalytic base with an unusually high pK_a value (pH 7.5), even though about 83% of the carboxyl group of Asp298 is estimated to be protonated at the pH of the crystallization buffer (pH 6.8; Chiu *et al.*, 2006). The side-chain atoms of Asp298 also have relatively large isotropic B factors (9.9–15.0 Å^2; average 11.4 Å^2). The side-chain conformation of Asn381, a strictly conserved residue in CuAOs, is clearly defined by a hydrogen bond between the ND2 atom of Asn381 and the main-chain carbonyl O atom of Val405 (Supplementary Fig. S5). The amide group of Asn381 is slightly tilted upwards at the OD1 atom against the plane of the TPQ ring, allowing the 'wedge-shaped' movement of TPQ during the catalytic process as described below.

The Cu-coordination structure in AGAO$_{PG}$ is identical to those reported previously (Wilce *et al.*, 1997; Kishishita *et al.*, 2003; Langley *et al.*, 2006). Namely, the Cu atom is coordinated by the N$^{\varepsilon 2}$ atoms of His431 and His433, the N$^{\delta 1}$ atom of His592 and two water molecules at the axial (Wat$_{ax}$) and equatorial (Wat$_{eq}$) positions in a distorted square-pyramidal geometry (Fig. 5). His592 can be modelled in two alternative conformations related by a rotation of ~65° around the C$^\alpha$—C$^\beta$ bond (Fig. 5). The occupancies of the two conformers (a and b) of His592 are 0.88 and 0.12, respectively, as in the previous AGAO structures, in which conformer a is always exclusive or preferential (Wilce *et al.*, 1997; Kishishita *et al.*, 2003; Langley *et al.*, 2006). It should be noted that the electron density modelled as the minor conformer b partially overlaps with that of pentaethyleneglycol [HO—(CH$_2$CH$_2$—O)$_n$—H, n = 5] bound close to this region (between the active site and the lake; occupancy = 0.48), suggesting that the pentaethyleneglycol molecule is bound in this site when His592 is in conformer a. The isotropic B factors of the Cu-coordinating N atoms of His431, His433 and conformers a and b of His592 (7.8, 8.9, 9.6 and 5.7 Å^2, respectively) were comparable to that of the Cu atom (9.9), although those of the O atoms of Wat$_{eq}$ and Wat$_{ax}$ (20.4 and 15.3 Å^2, respectively) were significantly higher.

3.5. Anisotropic displacement fluctuations

The anisotropic displacement parameters, which were accurately refined based on the high-resolution structure, indicate no significant correlated motion among the D2, D3 and D4 domains (not shown). However, by close inspection of the anisotropies of side-chain atoms that are relatively distant from the bound LMW PEG molecules, we noted characteristic thermal motions of the active-site residues which may be correlated with their movement during the catalytic reaction.

All of the side-chain atoms of Asp298, TPQ and Asn381 exhibited similar thermal ellipsoids, which tilt by about 60° from the vertical axis of the plane of the TPQ ring (Fig. 6), suggesting that these atoms are allowed to fluctuate coherently in the same or the opposite direction. The direction of this thermal fluctuation nearly coincides with the wedge-shaped movement of the TPQ ring that is proposed to occur in the reductive half-reaction of the catalytic reaction (Supplementary Fig. S5; Chiu *et al.*, 2006; Murray *et al.*, 1999). The

side-chain atoms of the conserved Asn381, which plays a crucial role in maintaining the balance of cofactor mobility *versus* rigidity that is expected to be necessary during the dual processes of cofactor biogenesis and catalysis, respectively (Schwartz *et al.*, 1998), are positioned ~3.5 Å above the TPQ ring and appear to serve as a 'cushion' for the TPQ ring by bending in the same direction as the wedge-shaped movement. Furthermore, Asn381 prevents TPQ from flipping out from the off-copper conformation, presumably by a weak NH–π interaction (Biot *et al.*, 2002), in cooperation with the strong hydrogen bond between TPQ and Tyr284 described above. The side-chain atoms of the conserved Asp298 also should move along with the wedge-shaped movement of TPQ to achieve efficient proton abstraction from the substrate Schiff base (Chiu *et al.*, 2006).

Additionally, the Cu atom and its ligands (His431, His433, His592, Wat_{eq} and Wat_{ax}) show anisotropic displacement fluctuations similar to those of Asp298, TPQ and Asn381 in magnitude and direction (Fig. 6). Although it is controversial whether the bound copper(II) atom plays a direct inner-sphere role or an indirect outer-sphere role in the re-oxidation of reduced TPQ by O_2 depending on the source of the CuAO (Smith *et al.*, 2010; Mukherjee *et al.*, 2008), a recent kinetic and spectroscopic study has demonstrated that the bound copper(II) atom in AGAO mediates electron transfer to O_2 through the copper(I)-semiquinone intermediate (direct inner-sphere mechanism; Shepard *et al.*, 2008). We have also determined the crystal structure of AGAO anaerobically reduced with substrate and found that the TPQ in the copper(I)-semiquinone state is in the on-copper conformation (T. Okajima, unpublished results). It is therefore reasonable to assume that the thermal fluctuations of the Cu atom and its ligands are also synchronized with those of TPQ and the nearby residues. Collectively, the anisotropic displacement fluctuations of all of the active-site residues in the resting state
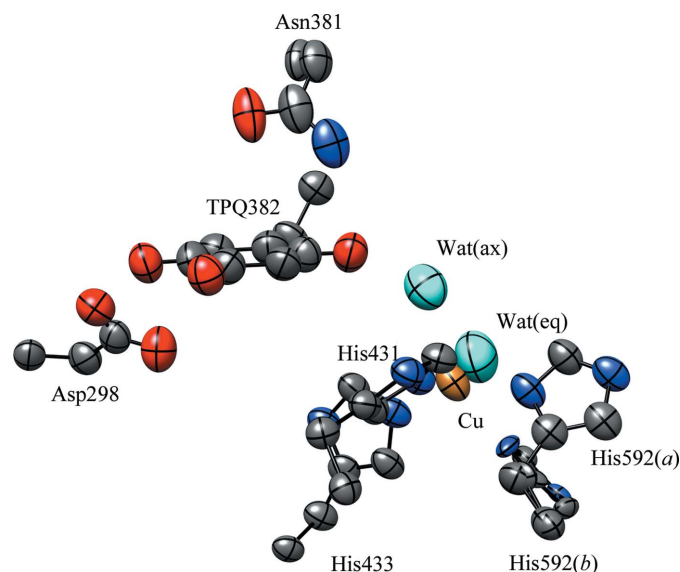
Figure 6
Distribution of anisotropic *B* factors. A magnified active-site view is shown with thermal ellipsoids represented at the 40% probability level.

reflect their coherent motions during the catalytic reaction and are markedly distinct from those of the remaining part of the whole molecule, in which the side-chain atoms of most residues have lower anisotropies or are in different orientations (Fig. 6).

3.6. Multiple conformers

We found that the number of residues identified to have multiple conformations depended on the resolution of the determined AGAO structures. Thus, although residues with multiple conformations were not found in the $AGAO_{RT}$ structure at 2.2 Å resolution (Wilce *et al.*, 1997) or in the $AGAO_{GL}$ structure at 1.8 Å resolution (Kishishita *et al.*, 2003) with the sole exception of the side chain of His592, which had two distinct conformers as described above, ten residues were modelled with two conformers in the $AGAO_{GL2}$ structure determined at 1.55 Å resolution (Langley *et al.*, 2006). In the present high-resolution $AGAO_{PG}$ structure, two residues have been modelled to have triple conformations (Arg263 with occupancies of 0.19, 0.55 and 0.26 in conformers *a*, *b* and *c*, respectively, and Ser569 with occupancies of 0.19, 0.58 and 0.23 in conformers *a*, *b* and *c*, respectively) and 73 residues to have dual conformations, which are located evenly in all of the domains (Supplementary Fig. S6). Among the ten residues modelled with two conformers in the $AGAO_{GL2}$ structure (Langley *et al.*, 2006), five residues (Ser21, Ile39, Glu143, His201 and Ile222) showed only a single conformation in the $AGAO_{PG}$ structure, most likely owing to conformational stabilization by LMW PEG molecules bound in the vicinity of these residues. It is noteworthy that Leu590 and Asp605, which constitute the anteroom (see below; Johnson *et al.*, 2007), have two conformers (Leu590 with occupancies of 0.36 and 0.64 in conformers *a* and *b*, respectively, and Asp605 with occupancies of 0.49 and 0.51 in conformers *a* and *b*, respectively), which would affect the size of the anteroom. In particular, the two conformers of Leu590 do not correspond to the major conformer in the xenon-bound AGAO structure (Duff *et al.*, 2004), in which the alkyl side chain should rotate nearly 180° around the $C^\alpha - C^\beta$ bond, suggesting that the anteroom of AGAO can only accommodate a Xe atom under a high pressure of Xe gas, with Leu590 being forced to take the third conformation (Supplementary Fig. S7).

4. Discussion

4.1. Effect of LMW PEG as a cryoprotectant

High-molecular-weight PEGs, such as PEG 2000 and PEG 4000, are frequently used as precipitants in protein crystallization buffers because of their significant dehydration effect, but are seldom employed as cryoprotectants, presumably owing to their molecular sizes and limited hydrophilic properties. In contrast, LMW PEG is moderately amphipathic, with hydrophilic hydroxyl groups at both ends separated by a short hydrophobic ethyl ether chain with high conformational flexibility. The molecular sizes of LMW PEGs are small enough to penetrate into the protein interior. These properties of LMW

PEG are considered to be advantageous for its use as a cryoprotectant. In addition, the LMW PEG used in this study is a mixture of different chain lengths [HO—(CH$_2$CH$_2$—O)$_n$—H with n (average) = 4.1], which can be accommodated in protein cavities of various sizes. Although soaking conditions must be carefully optimized because excess soaking of AGAO crystals with LMW PEG often causes deleterious damage (crystal cracking), LMW PEG should be widely applicable as a cryoprotectant for various protein crystals as a way to improve the X-ray diffraction quality.

### 4.2. Identification of bound O$_2$-like diatomic molecules

A notable finding in the present study is the identification of O$_2$-like diatomic molecules bound in the AGAO crystals prepared in a normal atmosphere. This is the first crystallographic identification of molecular oxygen bound to a CuAO in its resting state, showing that O$_2$ is able to bind to various parts of the enzyme that may serve as storage sites for the second substrate (O$_2$) during amine oxidation. Among the four identified diatomic molecules, three (Oxy1, Oxy2 and Oxy4) are replaced by water molecules in crystals grown in an N$_2$ atmosphere, suggesting that they are bound rather weakly to the protein. Nonpolar gases such as Xe have traditionally been used to explore molecular oxygen binding sites in hydrophobic cavities based on their hydrophobic features and similar size to dioxygen. However, hydrophilic oxygen-binding sites have also recently been discovered in cofactor-less oxidases and oxygenases using crystals under a high pressure of O$_2$ gas (Colloc'h et al., 2008) or crystals generated in a

solution containing a halide ion, which is employed as a mimic of molecular oxygen (Gabison et al., 2010; Roeser et al., 2007; Steiner et al., 2010). In the present high-resolution structure of AGAO$_{PG}$, the site that was presumed to be a consensus dioxygen (pre-)binding site (termed the 'anteroom'; Johnson et al., 2007) in previous structural studies using highly pressurized xenon gas (Lunelli et al., 2005; Duff et al., 2004; Johnson et al., 2007; Pirrat et al., 2008) is not occupied by an O$_2$-like diatomic molecule. Similarly, none of the four assigned O$_2$ (or N$_2$ for Oxy3) molecules is found in the sites where Xe atoms are bound in AGAO (Supplementary Fig. S8; Duff et al., 2004), suggesting that Xe binding does not necessarily reflect O$_2$ binding.

There are only a few cases where binding of O$_2$ at nonmetal sites has been observed in high-resolution protein structures: three O$_2$ molecules bound on the surface of the NG domain of the *Thermus aquaticus* Ffh protein (PDB entry 1ls1, 1.1 Å resolution; Ramirez et al., 2002) and one O$_2$ bound in the internal hydrophobic region of bacterial cholesterol oxidase (PDB entry 1mxt, 0.95 Å resolution; Lario et al., 2003). As in the AGAO crystals, O$_2$ molecules are bound to amino-acid side chains and water molecules via van der Waals and/or hydrogen-bonding interactions in these proteins.

4.3. Oxygen pathway to the active site

For all CuAOs, molecular oxygen is a common substrate in both cofactor biogenesis and catalysis. In catalysis, it participates in the oxidative half-reaction, in which the substrate-reduced TPQ is oxidized by molecular oxygen, yielding oxidized TPQ, ammonia and hydrogen peroxide. Two pathways that explain how O$_2$ migrates from the surrounding solvent to the buried active site have previously been proposed (Lunelli et al., 2005; Duff et al., 2004; Johnson et al., 2007). One involves migration from the central cavity (inland lake), where small molecules such as LMW PEG and O$_2$ can freely access the active site through several narrow openings via a short polar channel (Supplementary Figs. S1b and S1c; Wilce et al., 1997; Airenne et al., 2005; Lunelli et al., 2005; Duff et al., 2004). Another possible pathway is from either end of the β-sandwich in the D4 domain to the active site through the long hydrophobic region (Johnson et al., 2007; Pirrat et al., 2008). Common to both pathways, the end at the active site is around the anteroom, which has been proposed to be an oxygen pre-binding site (Johnson et al., 2007) and is composed mainly of hydrophobic residues (Ala400, Ala402, Phe435, Leu590, Asp605 and Val607 in AGAO; Supplementary Fig. S1c). Although the binding of O$_2$ in the proposed anteroom has not been observed in the present studies, Oxy2 is located closest to the anteroom and is in the channel from the inland lake to the active site. Thus, the 'pre-bound' O$_2$ in the Oxy2 site is well situated to be utilized as a substrate in the catalytic reaction, directly entering the active site (Fig. 7, blue dotted line). Alternatively, the O$_2$ may first migrate to the anteroom and then move to the active site before entering the active site itself (Fig. 7, red dotted line). However, some amino-acid residues constituting the anteroom, in particular Leu590 and
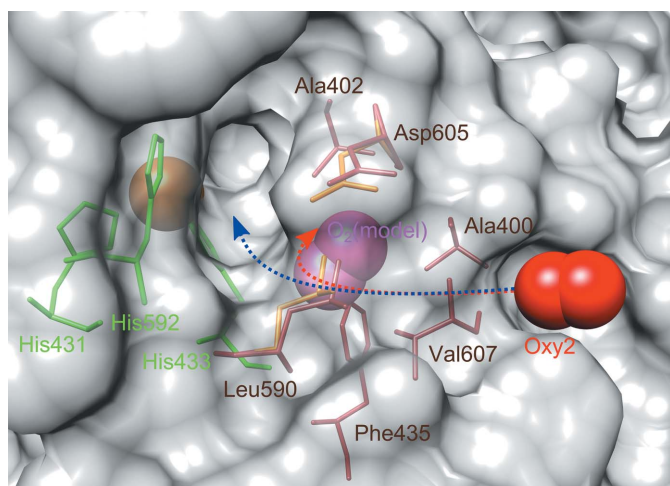
Figure 7
Proposed pathway of molecular oxygen entering from the Oxy2 site to the active site. Possible routes of molecular oxygen are represented by red and blue broken arrows. The molecular oxygen (Oxy2) and the Cu^{2+} ion are shown as red and orange spheres, respectively. An O$_2$ molecule is modelled in the anteroom on the basis of the Xe position in the AGAO–Xe structure (Duff et al., 2004) and is depicted as pink spheres. Three His residues (His431, His433 and His592) coordinating to Cu and the residues composing the anteroom are shown as green and brown sticks, respectively. Conformer *b* of Leu590 and Asp605 is shown in pale colours. Conformer *b* of His592 is not shown owing to its low occupancy. These and other residues are also shown as surface models in grey, excluding conformer *b* of Leu590 and Asp605.

Asp605, as already described, would undergo significant conformational changes in order to accommodate O_2 inside the limited space (3.2 to 3.6 Å in diameter with both Leu590 and Asp605 in conformers *b* and *a*, respectively); otherwise the modelled O_2 in the anteroom space appears to have van der Waals conflicts with the surrounding amino-acid side chains (Fig. 7).

In conclusion, our findings for the bound O_2-like diatomic molecules identified in the high-resolution crystal structure of the Cu/TPQ-containing AGAO suggest that the pathway of molecular oxygen to the active site in catalysis is most likely from the inland lake rather than from either end of the β-sandwich in the D4 domain. To study whether the same pathway is used in cofactor biogenesis, a high-resolution crystal structure of the Cu/TPQ-less precursor form of AGAO is also needed. Currently, efforts are under way in our laboratory to obtain good-quality crystals of the Cu/TPQ-less precursor form of AGAO using LMW-PEG as a cryoprotectant.

References

Adams, P. D. *et al.* (2010). *Acta Cryst.* D**66**, 213–221.

Airenne, T. T., Nymalm, Y., Kidron, H., Smith, D. J., Pihlavisto, M., Salmi, M., Jalkanen, S., Johnson, M. S. & Salminen, T. A. (2005). *Protein Sci.* **14**, 1964–1974.

Biot, C., Buisine, E., Kwasigroch, J. M., Wintjens, R. & Rooman, M. (2002). *J. Biol. Chem.* **277**, 40816–40822.

Brünger, A. T., Adams, P. D., Clore, G. M., DeLano, W. L., Gros, P., Grosse-Kunstleve, R. W., Jiang, J.-S., Kuszewski, J., Nilges, M., Pannu, N. S., Read, R. J., Rice, L. M., Simonson, T. & Warren, G. L. (1998). *Acta Cryst.* D**54**, 905–921.

Chen, V. B., Arendall, W. B., Headd, J. J., Keedy, D. A., Immormino, R. M., Kapral, G. J., Murray, L. W., Richardson, J. S. & Richardson, D. C. (2010). *Acta Cryst.* D**66**, 12–21.

Chiu, Y.-C., Okajima, T., Murakawa, T., Uchida, M., Taki, M., Hirota, S., Kim, M., Yamaguchi, H., Kawano, Y., Kamiya, N., Kuroda, S., Hayashi, H., Yamamoto, Y. & Tanizawa, K. (2006). *Biochemistry*, **45**, 4105–4120.

Choi, Y.-H., Matsuzaki, R., Fukui, T., Shimizu, E., Yorifuji, T., Sato, H., Ozaki, Y. & Tanizawa, K. (1995). *J. Biol. Chem.* **270**, 4712–4720.

Colloc'h, N., Gabison, L., Monard, G., Altarsha, M., Chiadmi, M., Marassio, G., Sopkova-de Oliveira Santos, J., El Hajji, M., Castro, B., Abraini, J. H. & Prangé, T. (2008). *Biophys. J.* **95**, 2415–2422.

Cona, A., Rea, G., Angelini, R., Federico, R. & Tavladoraki, P. (2006). *Trends Plant Sci.* **11**, 80–88.

Duff, A. P., Cohen, A. E., Ellis, P. J., Hilmer, K., Langley, D. B., Dooley, D. M., Freeman, H. C. & Guss, J. M. (2006). *Acta Cryst.* D**62**, 1073–1084.

Duff, A. P., Cohen, A. E., Ellis, P. J., Kuchar, J. A., Langley, D. B., Shepard, E. M., Dooley, D. M., Freeman, H. C. & Guss, J. M. (2003). *Biochemistry*, **42**, 15148–15157.

Duff, A. P., Trambaiolo, D. M., Cohen, A. E., Ellis, P. J., Juda, G. A., Shepard, E. M., Langley, D. B., Dooley, D. M., Freeman, H. C. & Guss, J. M. (2004). *J. Mol. Biol.* **344**, 599–607.

Emsley, P., Lohkamp, B., Scott, W. G. & Cowtan, K. (2010). *Acta Cryst.* D**66**, 486–501.

Gabison, L., Chiadmi, M., El Hajji, M., Castro, B., Colloc'h, N. & Prangé, T. (2010). *Acta Cryst.* D**66**, 714–724.

Harding, M. M. (2006). *Acta Cryst.* D**62**, 678–682.

Heras, B. & Martin, J. L. (2005). *Acta Cryst.* D**61**, 1173–1180.

Hernandez, M., Solé, M., Boada, M. & Unzeta, M. (2006). *Biochim. Biophys. Acta*, **1763**, 164–173.

Jalkanen, S., Karikoski, M., Mercier, N., Koskinen, K., Henttinen, T., Elima, K., Salmivirta, K. & Salmi, M. (2007). *Blood*, **110**, 1864–1870.

Janes, S. M., Mu, D., Wemmer, D., Smith, A. J., Kaur, S., Maltby, D., Burlingame, A. L. & Klinman, J. P. (1990). *Science*, **248**, 981–987.

Johnson, B. J., Cohen, J., Welford, R. W., Pearson, A. R., Schulten, K., Klinman, J. P. & Wilmot, C. M. (2007). *J. Biol. Chem.* **282**, 17767–17776.

Kim, M., Okajima, T., Kishishita, S., Yoshimura, M., Kawamori, A., Tanizawa, K. & Yamaguchi, H. (2002). *Nature Struct. Biol.* **9**, 591–596.

Kishishita, S., Okajima, T., Kim, M., Yamaguchi, H., Hirota, S., Suzuki, S., Kuroda, S., Tanizawa, K. & Mure, M. (2003). *J. Am. Chem. Soc.* **125**, 1041–1055.

Klema, V. J. & Wilmot, C. M. (2012). *Int. J. Mol. Sci.* **13**, 5375–5405.

Klinman, J. P. & Mu, D. (1994). *Annu. Rev. Biochem.* **63**, 299–344.

Kumar, V., Dooley, D. M., Freeman, H. C., Guss, J. M., Harvey, I., McGuirl, M. A., Wilce, M. C. & Zubak, V. M. (1996). *Structure*, **4**, 943–955.

Kyte, J. & Doolittle, R. F. (1982). *J. Mol. Biol.* **157**, 105–132.

Langley, D. B., Duff, A. P., Freeman, H. C. & Guss, J. M. (2006). *Acta Cryst.* F**62**, 1052–1057.

Lario, P. I., Sampson, N. & Vrielink, A. (2003). *J. Mol. Biol.* **326**, 1635–1650.

Li, R., Klinman, J. P. & Mathews, F. S. (1998). *Structure*, **6**, 293–307.

Lucero, H. A. & Kagan, H. M. (2006). *Cell. Mol. Life Sci.* **63**, 2304–2316.

Lunelli, M., Di Paolo, M. L., Biadene, M., Calderone, V., Battistutta, R., Scarpa, M., Rigo, A. & Zanotti, G. (2005). *J. Mol. Biol.* **346**, 991–1004.

Maintz, L. & Novak, N. (2007). *Am. J. Clin. Nutr.* **85**, 1185–1196.

Matsuzaki, R., Fukui, T., Sato, H., Ozaki, Y. & Tanizawa, K. (1994). *FEBS Lett.* **351**, 360–364.

Matsuzaki, R. & Tanizawa, K. (1998). *Biochemistry*, **37**, 13947–13957.

McCoy, A. J., Grosse-Kunstleve, R. W., Adams, P. D., Winn, M. D., Storoni, L. C. & Read, R. J. (2007). *J. Appl. Cryst.* **40**, 658–674.

McGrath, A. P., Hilmer, K. M., Collyer, C. A., Shepard, E. M., Elmore, B. O., Brown, D. E., Dooley, D. M. & Guss, J. M. (2009). *Biochemistry*, **48**, 9810–9822.

McGrath, A. P., Mithieux, S. M., Collyer, C. A., Bakhuis, J. G., van den Berg, M., Sein, A., Heinz, A., Schmelzer, C., Weiss, A. S. & Guss, J. M. (2011). *Biochemistry*, **50**, 5718–5730.

McIntire, W. S. & Hartmann, C. (1993). *Principles and Applications of Quinoproteins*, edited by V. L. Davidson, pp. 97–171. New York: Marcel Dekker.

Mukherjee, A., Smirnov, V. V., Lanci, M. P., Brown, D. E., Shepard, E. M., Dooley, D. M. & Roth, J. P. (2008). *J. Am. Chem. Soc.* **130**, 9459–9473.

Murakawa, T., Hayashi, H., Taki, M., Yamamoto, Y., Kawano, Y., Tanizawa, K. & Okajima, T. (2012). *J. Biochem.* **151**, 167–178.

research papers

Murakawa, T., Okajima, T., Kuroda, S., Nakamoto, T., Taki, M., Yamamoto, Y., Hayashi, H. & Tanizawa, K. (2006). *Biochem. Biophys. Res. Commun.* **342**, 414–423.

Murray, J. M., Saysell, C. G., Wilmot, C. M., Tambyrajah, W. S., Jaeger, J., Knowles, P. F., Phillips, S. E. & McPherson, M. J. (1999). *Biochemistry*, **38**, 8217–8227.

Murshudov, G. N., Skubák, P., Lebedev, A. A., Pannu, N. S., Steiner, R. A., Nicholls, R. A., Winn, M. D., Long, F. & Vagin, A. A. (2011). *Acta Cryst.* D**67**, 355–367.

Okajima, T. & Tanizawa, K. (2009). *Copper Amine Oxidases: Structures, Catalytic Mechanisms and Role in Pathophysiology*, edited by G. Floris & B. Mondovì, pp. 113–118. Boca Raton: CRC Press.

Otwinowski, Z. & Minor, W. (1997). *Methods Enzymol.* **276**, 307326.

Parsons, M. R., Convery, M. A., Wilmot, C. M., Yadav, K. D., Blakeley, V., Corner, A. S., Phillips, S. E., McPherson, M. J. & Knowles, P. F. (1995). *Structure*, **3**, 1171–1184.

Pettersen, E. F., Goddard, T. D., Huang, C. C., Couch, G. S., Greenblatt, D. M., Meng, E. C. & Ferrin, T. E. (2004). *J. Comput. Chem.* **13**, 16051612.

Pirrat, P., Smith, M. A., Pearson, A. R., McPherson, M. J. & Phillips, S. E. V. (2008). *Acta Cryst.* F**64**, 1105–1109.

Ramirez, U. D., Minasov, G., Focia, P. J., Stroud, R. M., Walter, P., Kuhn, P. & Freymann, D. M. (2002). *J. Mol. Biol.* **320**, 783–799.

Roeser, D., Schmidt, B., Preusser-Kunze, A. & Rudolph, M. G. (2007). *Acta Cryst.* D**63**, 621–627.

Sabu, A., Kondo, S., Saito, R., Kasai, Y. & Hashimoto, K. (2005). *J. Phys. Chem. A*, **109**, 1836–1842.

Schulz, E. C., Neumann, P., Gerardy-Schahn, R., Sheldrick, G. M. & Ficner, R. (2010). *Acta Cryst.* D**66**, 176–180.

Schwartz, B., Green, E. L., Sanders-Loehr, J. & Klinman, J. P. (1998). *Biochemistry*, **37**, 16591–16600.

Shepard, E. M., Okonski, K. M. & Dooley, D. M. (2008). *Biochemistry*, **47**, 13907–13920.

Smith, M. A., Pirrat, P., Pearson, A. R., Kurtis, C. R., Trinh, C. H., Gaule, T. G., Knowles, P. F., Phillips, S. E. & McPherson, M. J. (2010). *Biochemistry*, **49**, 1268–1280.

Steiner, R. A., Janssen, H. J., Roversi, P., Oakley, A. J. & Fetzner, S. (2010). *Proc. Natl Acad. Sci. USA*, **107**, 657–662.

Taki, M., Murakawa, T., Nakamoto, T., Uchida, M., Hayashi, H., Tanizawa, K., Yamamoto, Y. & Okajima, T. (2008). *Biochemistry*, **47**, 7726–7733.

Wilce, M. C., Dooley, D. M., Freeman, H. C., Guss, J. M., Matsunami, H., McIntire, W. S., Ruggiero, C. E., Tanizawa, K. & Yamaguchi, H. (1997). *Biochemistry*, **36**, 16116–16133.

Winn, M. D. *et al.* (2011). *Acta Cryst.* D**67**, 235–242.